iScience

CellPress

Article

A High-Throughput Small Molecule Screen Identifies Ouabain as Synergistic with miR-34a in Killing Lung Cancer Cells

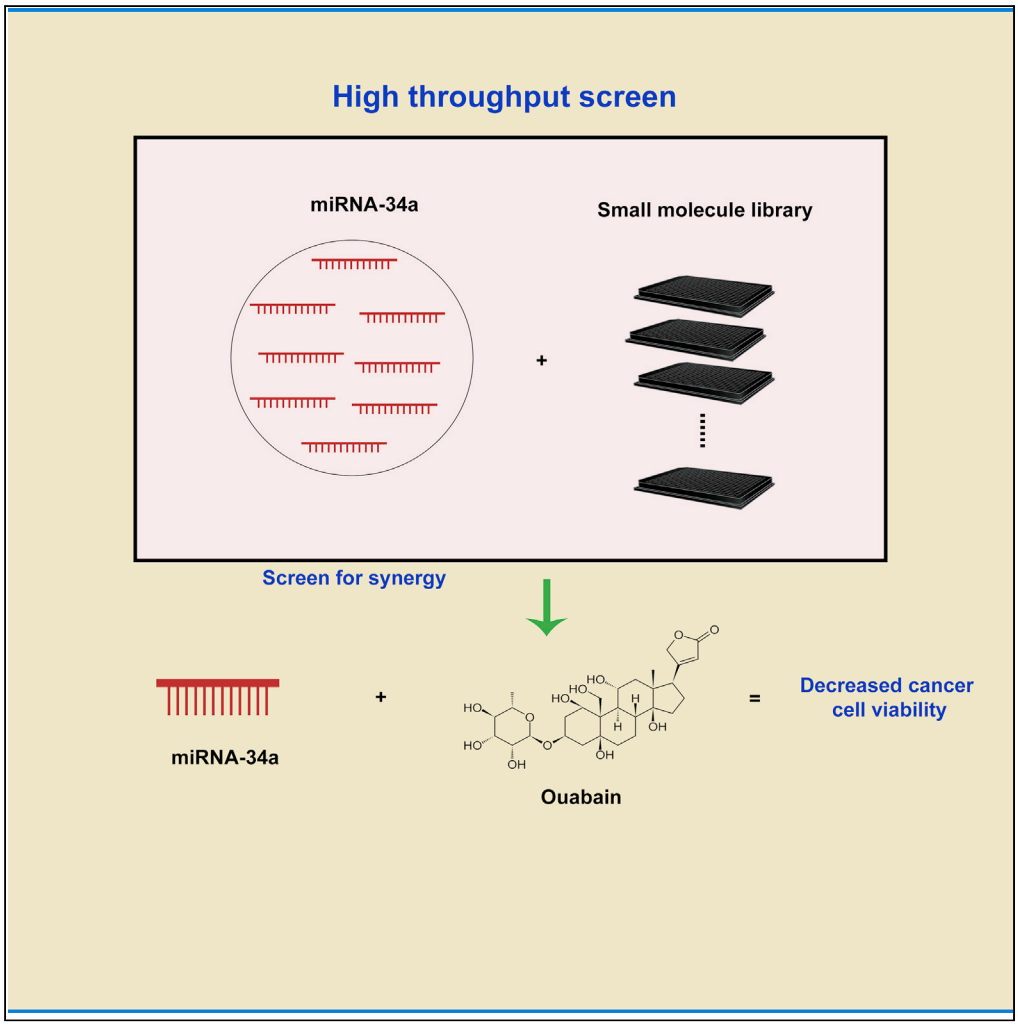

Rajesha Rupaimoole, Bohyung Yoon, Wen Cai Zhang, Brian D. Adams, Frank J. Slack

fslack@bidmc.harvard.edu

HIGHLIGHTS

miR-34a is a tumor suppressor miRNA downregulated in many cancers including lung cancer

Screen identifying small molecule-miR-34a combinations against cancer cells established

Small molecule ouabain acts in synergy with miR-34a to kill cancer cells

Autophagy signaling was observed upon treatment of cancer cells with ouabain and miR-34

Rupaimoole et al., iScience *23*, 100878
February 21, 2020
https://doi.org/10.1016/j.isci.2020.100878

iScience

CellPress

Article

A High-Throughput Small Molecule Screen Identifies Ouabain as Synergistic with miR-34a in Killing Lung Cancer Cells

Rajesha Rupaimoole,[1,2] Bohyung Yoon,[1] Wen Cai Zhang,[1,3] Brian D. Adams,[1,4] and Frank J. Slack[1,5,*]

SUMMARY

MicroRNA-34 (miR-34) is one of the major families of tumor suppressor miRNAs often lost in cancers. Delivery of miR-34a mimics to affected tumors as a therapeutic strategy has been tried in pre-clinical studies and in a phase I clinical trial. One approach to increase efficacy and reduce toxicity is to rationally identify drug combinations with small molecules that synergize with miR-34a. In this study we performed a high-throughput screen of a large panel of small molecules with known biological activity and identified ouabain as a candidate small molecule that synergized with miR-34a in killing lung cancer cells. We elucidated autophagy activation as a key mechanism by which miR-34a and ouabain causes increased cytotoxicity in cells. We posit that this combinatorial approach could reduce the active dose of miR-34a needed *in vivo* to observe tumor shrinkage and potentiate the development of miR-34a combination therapies in the future.

INTRODUCTION

Lung cancer has the number one mortality among all cancer types with an estimated number of deaths of 140,000 in year 2019 in the United States (Siegel et al., 2019). The majority of patients are diagnosed with non-small cell lung cancer (NSCLC) and have aggressive metastasis and resistance to existing therapeutics. Novel therapeutic strategies based on rational drug combinations to overcome drug resistance is currently needed in the clinic. Of the family of noncoding RNAs (ncRNAs), microRNAs (miRNAs) exist as small ncRNAs and mediate target translational inhibition or degradation by binding to complementary regions in target mRNAs (Peng and Croce, 2016; Rupaimoole and Slack, 2017). Since the discovery of the first miRNA in 1993 and 7 years later the first mammalian miRNA, *let-7*, currently more than 2,000 human miRNAs have been discovered (Bartel, 2004; Reinhart et al., 2000). These miRNAs have been shown to regulate key cell signaling events such as apoptosis, proliferation, migration, and differentiation. Considering the widespread roles of miRNAs in cell biology, it is not surprising that a significant number of these miRNAs play roles in cancer progression (Bartel, 2004; Rupaimoole and Slack, 2017). One such miRNA, miR-34a, is often downregulated in cancers and involved in oncogenic programming of cancer cells (Chang et al., 2007; Li et al., 2013; Liu et al., 2011). Transcription of miR-34a is regulated by p53 binding to the promoter region of miR-34a and activating its transcription (Chang et al., 2007). Major cancers such as lung and pancreatic cancers have shown to exhibit downregulation of miR-34a (Rupaimoole and Slack, 2017). miR-34a has been shown to play roles in DNA damage response-mediated apoptosis by direct targeting of Sirtuin 1(Li et al., 2013). Numerous studies have shown a role for miR-34a as a tumor suppressor miRNA via targeting several cell cycle proteins such as CDK4/6, anti-apoptosis proteins such as BCL2, and metastasis-related proteins such as MYC and CD44 (Misso et al., 2014).

In recent years, several preclinical studies have shown the potential for tumor suppressor miRNA replenishment as a viable therapeutic against cancers. Along this line, miR-34a replenishment therapy is one of the most widely tested miRNA strategies and has advanced to a phase I clinical trial against several solid and hematological malignancies (Bader, 2012). In models of NSCLC, a liposomal formulation of miR-34a mimic was delivered to xenografted lung tumors and significant inhibition of tumor growth was observed (Trang et al., 2011). Furthermore, tumors expressed lower levels of proteins that are regulated by miR-34a, such as MET and BCL2. In the $Kras^{LSL-G12D/+}$;$Trp53^{LSL-R172H/+}$ model of NSCLC, which is highly resistant to anticancer therapies, viral vector-based and nanoparticle strategies to deliver inducible miR-34a also showed promise by decreasing tumor burden and targeting Bcl2 protein reduction (Kasinski and Slack, 2012; Kasinski et al., 2015). Recently, miR-34a encapsulated in an early-generation lipid nanoparticle was tested in a clinical trial, and unfortunately, during the dose escalation stage, a small number of patients

[1]HMS Initiative for RNA Medicine and Department of Pathology, Harvard Medical School, Beth Israel Deaconess Medical Center, Boston, MA 02215, USA

[2]Present address: SHEPHERD Therapeutics, Natick, MA 01760, USA

[3]Present address: Cancer Division, Burnett School of Biomedical Sciences, University of Central Florida College of Medicine, Orlando, FL 32827, USA

[4]Present address: Department of RNA Science, The Brain Institute of America, New Haven, CT 06511, USA

[5]Lead Contact

*Correspondence: fslack@bidmc.harvard.edu

https://doi.org/10.1016/j.isci.2020.100878

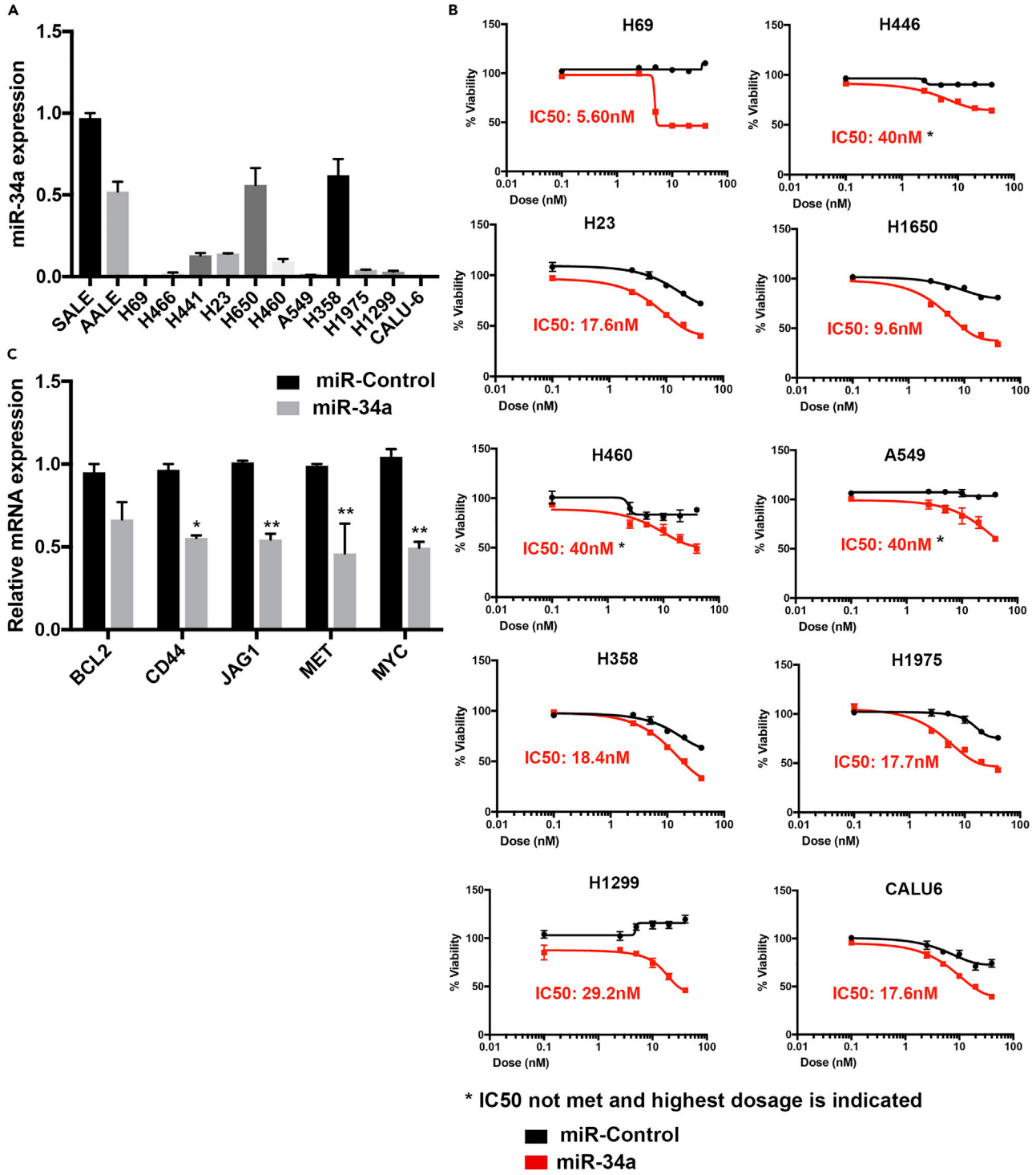

Figure 1. Evaluation of miR-34a Expression and Dependence in a Panel of Lung Cancer Cell Lines

(A and B) (A) Distribution of miR-34a expression in non-small cell lung cancer cell lines compared with normal lung epithelial cells SALE and AALE. Compared with SALE, all cancer cell lines showed a significant reduction in miR-34a levels ($p < 0.001$), and compared with AALE, except for H650 and H358, all the cancer cell lines showed a significant reduction in miR-34a levels ($p < 0.001$). (B) miR-Control and miR-34a dose-response curves in non-small cell lung cancer cell lines ($n = 10$). Cells were transfected with miR-Control or miR-34a for 72 h, and viability was measured using the MTT reagent.

Figure 1. *Continued*

(C) Data showing qPCR-based measurements of miR-34a downstream genes *BCL2*, *CD44*, *JAG1*, *MET*, and *MYC*, after treating A549 cells with miR-Control and miR-34a mimics at 40 nM for 72 h. All comparisons are done with respective miR-Control gene expression (*$p < 0.05$, **$p < 0.005$, Student's t test). Bars and errors bars represent the means and the corresponding SEMs for $n \geq 3$.

showed immune-related cytotoxicity and the trial ended (Beg et al., 2015). The cause of the toxicity is unknown, but this issue reiterates the need for careful consideration of dosing and targeted therapeutics using nanoparticles with ligands to cancer cell receptors, avoiding off-target cytotoxicity or adversarial immune reactions.

In this current study we take a novel approach in an attempt to increase miR-34a therapeutic efficiency by identifying a possible combination therapy with small molecules. Using a high-throughput screen consisting of ~10,000 small molecules of known biological activity, we identify ouabain as a top small molecule candidate to combine synergistically with miR-34a in killing lung cancer cells. We believe that the combination approach will help in reducing the effective dose for miR-34a needed in the clinic and could allow for a reduction in adverse reactions.

RESULTS AND DISCUSSION

A Screen of Lung Cancer Cells for miR-34a Sensitivity

Previous studies have shown that miR-34a induces apoptosis and reduces tumor growth in many cancer cell types, and lung cancer is one of the major cancer types among them. First, we measured miR-34a expression in a panel of lung cancer cell lines (n = 11) and compared this with immortalized lung epithelial cells SALE and AALE. We observed that, compared with AALE and SALE cells, many NSCLC cells have low expression of miR-34a, with A549 being one of the least expressing cells (Figure 1A). To understand how these cells respond to miR-34a expression rescue, we artificially introduced miR-34a in these cells using miR-34a mimics. All of the cell lines showed decreased viability in the miR-34a-treated group compared with miR-Control, as measured by MTT assay (Figure 1B). Interestingly the IC50 values did not correlate with their basal miR-34a expression and the IC50 ranged from 5.60 to 40 nM, the highest of the tested doses (Figure 1B). We selected A549 cells for establishing a high-throughput screen based on observation that this cell line has low expression of miR-34a and is partially resistant to miR-34a rescue. This would provide a window to improve miR-34a therapy in combination with a small molecule. Furthermore, in A549 cells we tested the effect on expression of miR-34a downstream targets *BCL2*, *CD44*, *JAG1*, *MET*, *MYC* and observed that the majority of these downstream targets showed significant reductions in mRNA expression (Figure 1C). This further confirmed that A549 cells respond to miR-34a treatment and act as a suitable cell line for establishing a small molecule enhancer screen.

Establishing a Cell-Based System for miR-34a Enhancement

The doxycycline inducible expression system has been used widely in studies to control gene expression and perform investigations in a controlled manner. For the current study to screen small molecules acting synergistic with miR-34a, we established A549 cells with inducible overexpression of miR-34a. We cloned the miR-34a coding sequence into a lentiviral plasmid with TET response element adjacent to the promoter. Lentiviral particles were transduced into A549 cells, and we measured expression of miR-34a after addition of doxycycline (Figure 2A). Our data showed a dose-dependent increase in miR-34a expression at the 72-h time point (Figure 2B). We selected 1 mg/mL as a dose of doxycycline for subsequent experiments as this dose induced miR-34a level comparable with those found in the normal lung cell lines screened as per Figure 1A (for example, A549 cells showed ~350-fold lower miR-34a compared with the average of SALE and AALE expression). We confirmed activity of induced miR-34a using a reporter plasmid containing miR-34a target sequence placed in the 3′ UTR region of luciferase. Our data showed a significant decrease in luciferase signal upon induction with doxycycline at 1 mg/mL for 72 h (Figure 2C), confirming active miR-34a in A549 cells. Upon checking mRNA expression of miR-34a downstream targets, CD44 and SRC, our data showed a significant reduction at the 48- and 72-h time points, confirming that miR-34a is active in downstream signaling modulation (Figure 2D).

High-Throughput Assay Standardization for the Screen of Small Molecules to Combine Synergistically with miR-34a

For the phenotypic assay, we used detection of apoptosis induction (by measuring activated caspase 3) and the total number of cells (using Hoechst nuclear staining). Optimization of cell numbers and the HT

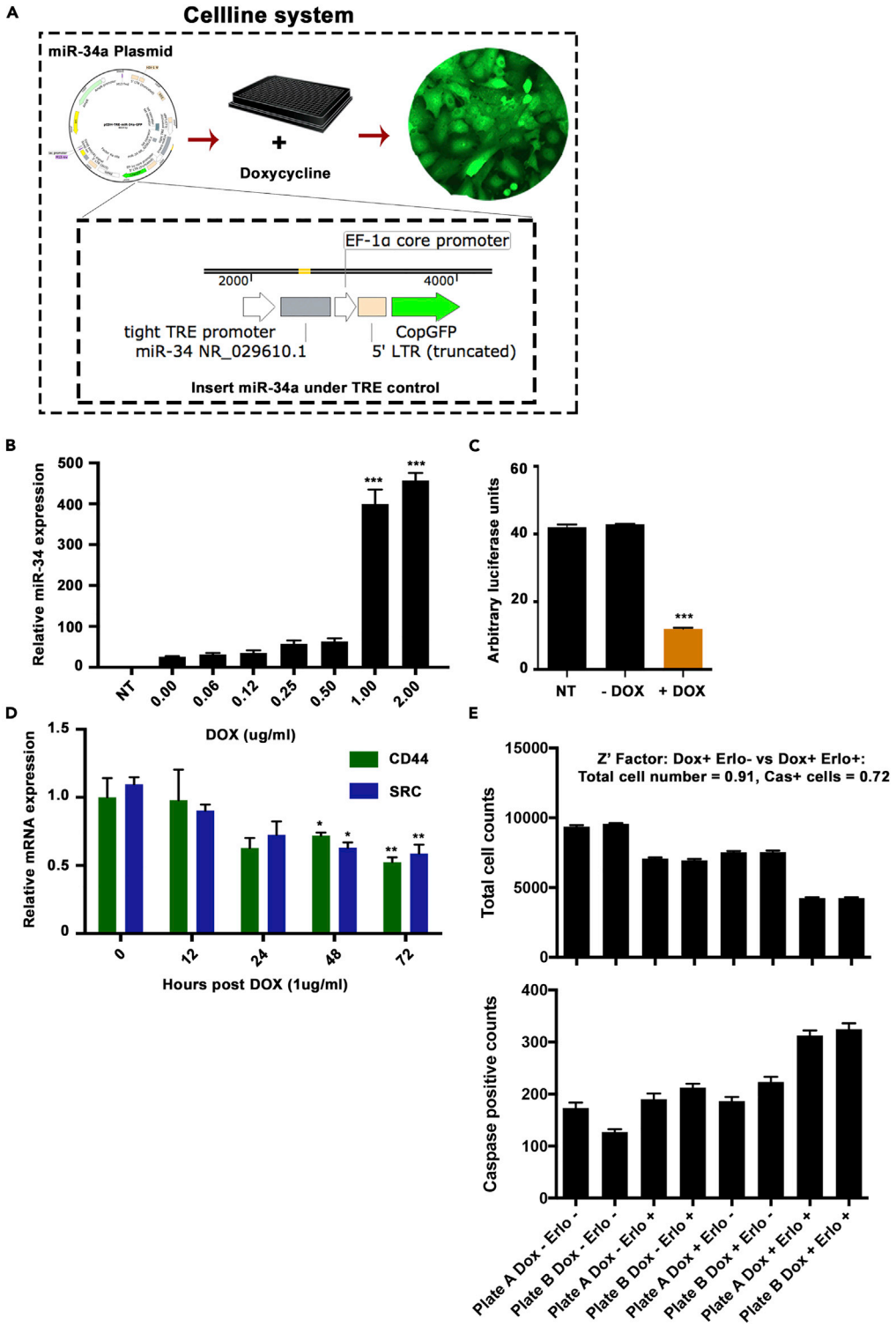

Figure 2. Establishing the miR-34a Inducible Expression System and an Assay for the Small Molecule Screen

(A) Schematic of the cell line system for miR-34a expression inducible by adding doxycycline. The miR-34a pre-miRNA was placed next to a TET responsive element, and CopGFP was placed under control of EF1a core promoter. Cells were selected for GFP expression and used in downstream assays.

Figure 2. *Continued*

(B) Expression of miR-34a in A549-miR-34a cells after adding increasing doses of doxycycline (DOX) for 48 h (***$p < 0.005$, Student's t test).

(C) miR-34a reporter luciferase activity upon addition of doxycycline at 1 μg/mL dose to A549-miR-34a cells, compared with non-transfected (NT) cells or without DOX, time point set to 48 h (***$p < 0.005$, Student's t test).

(D) Expression of miR-34a downstream genes *CD44* and *SRC* after inducing miR-34a expression using DOX at 1 μg/mL treatment with time course monitored up to 72 h (*$p < 0.05$, **$p < 0.01$, Student's t test). Bars and errors bars represent the means and the corresponding SEMs for $n \geq 3$.

(E) Establishing the cell-based assay for detection of total cell counts and caspase 3-activated cells. DOX and Erlotinib were added to a set of A549-miR-34a cells plated in parallel, and total cell numbers and activated caspase 3-positive cell counts were taken, followed with data analysis to measure the Z-factor.

assay was performed using A549-miR34 cells with a positive control compound, erlotinib, as previously we had seen combining miR-34a with erlotinib treatment showed a decrease in IC50 *in vitro* (Stahlhut and Slack, 2015). An initial cell number screen showed that the optimal cell number in 384-well plates to show increased caspase activity and a significant decrease in cell numbers is 5,000 cells. Images showed a consistent increase in caspase 3 fluorescence signal in erlotinib treated or doxycycline combination groups (Figures S1A and S1B). Furthermore, the robustness of the established assay was measured using cells plated in 384-well plates in conditions similar to the small molecule screen conditions and signals were measured using an automated plate reader with robotic handling of plates. Data analysis for the Z factor showed a valid score of 0.91 for total cell count and 0.72 for caspase 3 + cells (Figure 2E). For all screening plates, the quality control Z factor was set to 0.5, and any plates below this threshold, were repeated.

Ouabain Sensitizes Lung Cancer Cells to miR-34a Treatment

Upon finalizing the phenotypic assay, cells with miR-34a induction were screened with 9,908 bioactive compounds (Table S1, Figures S2A and S2B) for increased apoptosis and decreased cell numbers. XY plot of +dox versus −dox readouts with all the molecules ($n = 9,908$) screened showed linearity and confirmed the robustness of the assay (Figure 3A). Furthermore, positive control erlotinib treatment points showed a shift toward the +dox axis in % caspase activity and shift toward −dox axis with respect to total cell counts, verifying the validity of the assay and the data generated. Data from the small molecule screen for % decrease in cell numbers and caspase + cells was used for initial stratification of top candidates to be subsequently tested in a cherry pick screen (Figures 3B and Table S2). For the cherry pick screen, we included the top 48 molecules (two of fifty molecules were omitted as they belonged to the same family) from the initial screen and a six-point dose-response curve was plotted starting with the maximum feasible dose (IC50s and caspase 3-positive cells data are in Table S2). Our data showed similarity to the initial screen, and molecules repeated in terms of cell number decrease and increased caspase + cells upon miR-34a inductions. However, several of the 50 molecules did not reach an IC50 at the highest dose in control cells or miR-34a-induced cells; hence we used IC30 for selecting the next set of top candidates to move into combination index calculations with miR-34a transfections in multiple cell lines.

Based on our stringent criteria of decrease in IC30 (median 72% as cut off) and increased caspase-positive cells, we selected seven candidates from Table S3 for conducting Lowe's additivity combination index synergy analysis. Increasing doses of the top seven drugs in A549 and HCC827 cells, with increasing doses of miR-34a mimic transfection, were used. miR-Control was used to measure any cytotoxicity arising from transfection or drug class. Our data showed a maximum synergetic score and points in the matrix for ouabain followed by QNZ (Figures3C, S3A, and S2B). Furthermore, this synergy was not observed in miR-Control-treated combinations suggesting a role of miR-34a in causing synergistic decreases in viability as measured through total cell counts. We confirmed the observed synergy by using an MTT assay for viability in four lung cancer cell lines with varying mutational landscape A549, HCC827, H1975, and CALU6. Our data showed a significant shift in IC50 in all four cell lines and confirmed the role of ouabain in causing a synergistic decrease in viability with miR-34a treatment (Figure 3D).

Ouabain and miR-34a Combination Effects Are Seen in Pancreatic and Colon Cancer Cells and Patient-Derived Xenografts from Lung Cancer Patient

Considering that miR-34a is lost in many other cancers including pancreatic and colon cancers, we further explored the applicability of findings from this study to these cancers. We used the BXPC3 cell line for

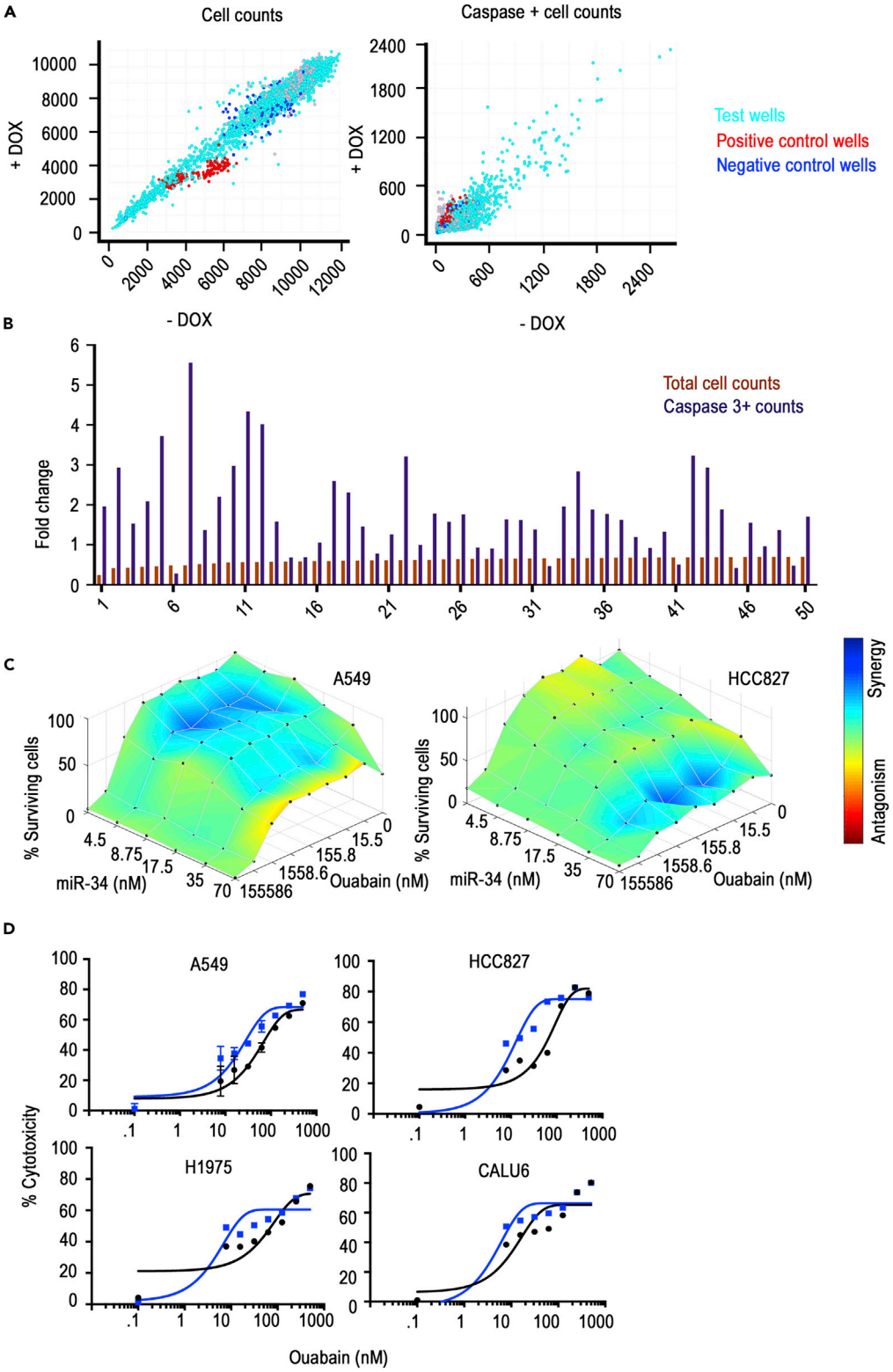

Figure 3. High-Throughput Screen Identification of the miR-34a Synergistic Small Molecule Ouabain

(A) Data show XY plots with cell counts and activated caspase 3 + cells in doxycycline-treated (DOX+) versus control cells (DOX−). Data summarized from 9,850 small molecules of biologically known activity.

Figure 3. *Continued*

(B) Plot of fold change in total cell counts and caspase 3 + cell counts from cells treated with doxycycline compared with control untreated cells. Data from the top 50 molecules with decreased cell numbers and increased caspase 3 + cells are shown.

(C) Synergy plot of miR-34a and ouabain-treated A549 and HCC827 lung cancer cells. Lowe's additivity combination index was calculated and plotted as heatmap using Combenefit data analysis tool.

(D) MTT assay-based validation of the observed synergy with ouabain and miR-34a in A549, HCC827, H1975, and CALU6 lung cancer cells. Data show % cytotoxicity in 40 nM miR-34a treated (blue line) versus 40 nM miR-control (black line) with an increasing dose of ouabain. Data were fitted by non-linier regression with variable slope. Goodness of fit showed R squared for all the IC50 plots greater than 0.9.

pancreatic cancer and HCT116 and HCT15 cells for colon cancer. Our data with three different doses of ouabain showed a significant decrease in cell counts compared with control or individual ouabain, or miR-34a treatments (Figure 4A).

Patient-derived xenograft and primary 3-dimensional cell cultures (organoids) have been recently used in studies and are suggested to be closer to *in vivo* models than 2D cell cultures. In our current study we utilized such a system and established 3D patient-derived lung cancer spheroids embedded in low concentration of geltrex mixed in cell culture media. miR-Control-treated group showed normal growth of spheroids, and miR-34a or ouabain treatment resulted in a decreased number of spheroids (Figure 4B). However, the largest significant decrease was observed in miR-34a and ouabain-treated cells consistent with the monolayer cell culture findings above (Figure 4B).

Ouabain Acts Synergistically with miR-34a via Induction of Autophagy

During the course of study, we noticed that cells treated with ouabain showed a large number of vacuoles and this number increased in combination with miR-34a (Figure 5A). A comparison of our phase contrast images with those found in the literature indicated that the clear morphology changes we observed were consistent with autophagy (Parzych and Klionsky, 2014). To test this, cells were transduced with the Premo Autophagy Tandem Sensor RFP-GFP-LC3B system to study the definitive molecular changes related to autophagy. This sensor has an acid-sensitive GFP signal and acid-insensitive RFP signal upon induction of autophagy in cells. In the ouabain treatment group we observed increased autophagolysosome- (RFP) and autophagosome- (GFP) positive cells compared with control or miR-34a treatments (Figure 5B). Western blots of lysates from cells treated with miR-control, ouabain, miR-34a, and the combination showed increased LC3A/B signal and confirmed induction of autophagy (Figure 5C). All of these data suggested activation of autophagy and associated cell death when cells are treated with miR-34a and ouabain.

Conclusion

Of several hundred miRNAs identified in humans, a few have emerged as strong tumor suppressors, often lost owing to deregulation in the transcription machinery regulating particular miRNAs (Bartel, 2004; Rupaimoole and Slack, 2017). One such miRNA is miR-34a, directly downstream of the p53 transcription factor (Chang et al., 2007). Loss of p53 and related loss of expression of miR-34a has been reported in many cancers including lung cancer (Chang et al., 2007). Reintroduction of tumor suppressor miRNAs has shown therapeutic efficacy against cancers, and miR-34a has progressed past preclinical studies into clinical trials (Kasinski and Slack, 2012; Trang et al., 2011). In addition to delivery of miR-34a using nanoparticles, a preclinical study recently showed use of ligand-mediated *in vivo* delivery of miR-34a (Orellana et al., 2017). MRX34, a clinical formulation of miR-34a in nanoliposomes had shown significant hepatic tumor reduction in *in vivo* xenograft studies (Beg et al., 2015). Despite mostly manageable safety in the dose escalation phase of the early phases of the clinical trial, three patients developed immune-related serious adverse events and the trial was halted. This suggests that, despite the attractive promise of single agent miRNA therapy, there is a need for combination therapeutics, potentially decreasing the need for large single-dose compounds. In this study we screened ~10,000 biologically active compounds for their potential to induce cell killing in combination with miR-34a in a synergistic manner. With multiple experimental validations, we identified ouabain as a small molecule capable of inducing significant cell killing even at low doses of ouabain and miR-34a.

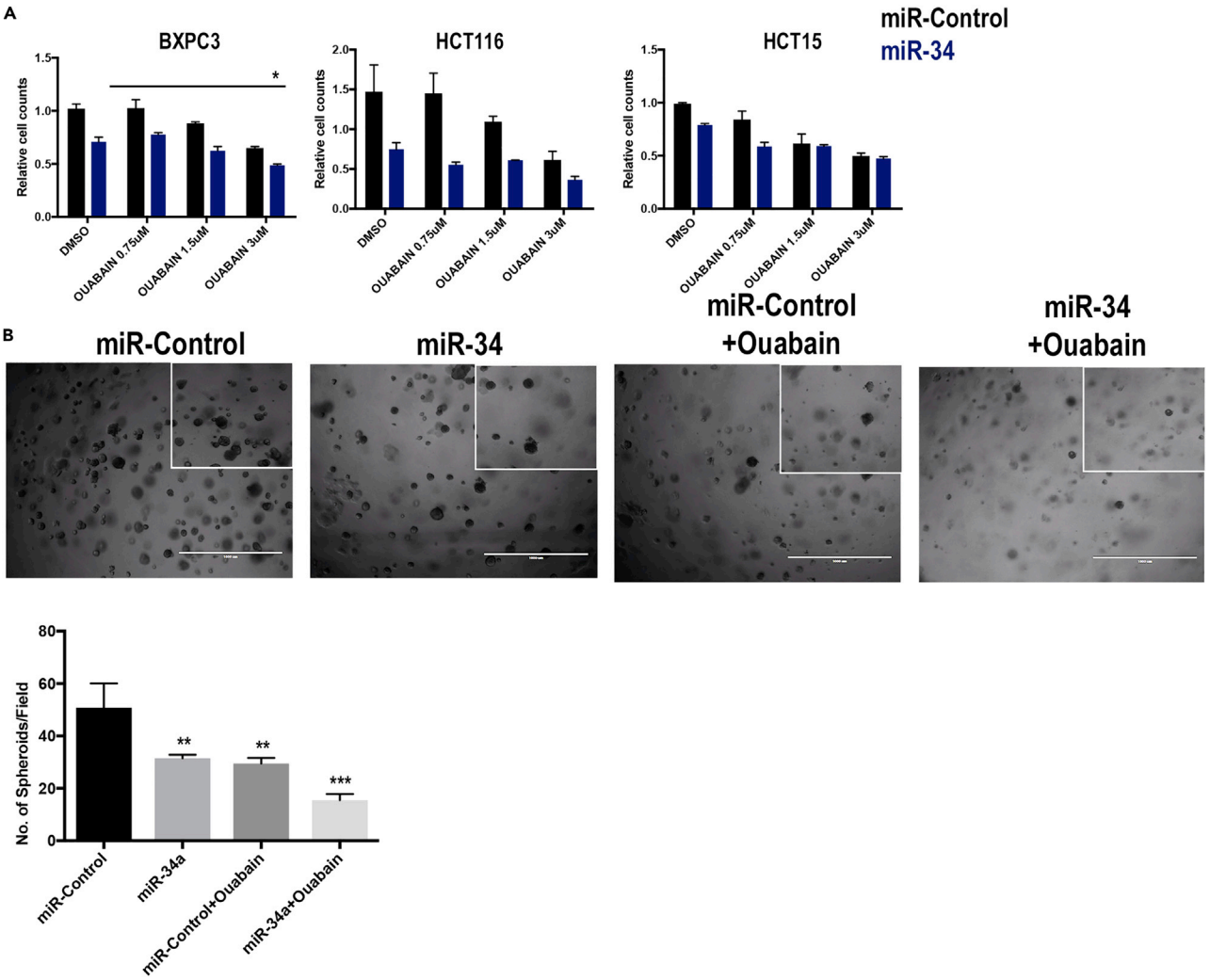

Figure 4. Testing of Synergy between Ouabain and miR-34a in Additional Cancer-Type Cells and Lung Cancer Patient-Derived Xenograft (PDX) 3D Cell Cultures

(A) Data showing a change in cell counts after treating cells with increasing doses of ouabain and miR-34a at 40 nM concentration in pancreatic BXPC3 and colon cancer HCT116 and HCT15 cells. Upon using ANOVA with multiple comparison test, only BXPC3 showed significance between miR-34a and miR-34a with ouabain at 3-μM dose (*$p < 0.05$) (B) Primary cultures established from a lung cancer patient-derived xenograft were treated with miR-34a or a combination of miR-34a and ouabain. The number of spheroids is quantified in the bottom panel (**$p < 0.01$, ***$p < 0.001$, Student's t test). Bars and errors bars represent the means and the corresponding SEMs for $n \geq 3$.

Previous studies have shown a role for ouabain and related cardiac glycosides in inducing cancer cell apoptosis mediated by direct inhibition of Na^+ K^+ ATPases (Cherniavsky-Lev et al., 2014). Inhibition of ATPases resulted in induction of apoptosis via activation of JNK leading to decreased Bcl2 and releasing Beclin1, an autophagy inducer (Trenti et al., 2014). In parallel to this study, our data suggest that, upon combination with miR-34a, LC3 production and cleavage, definitive markers of autophagy were increased. Furthermore, these data directly correlate with decreased cell viability and increased apoptosis measured via Caspase 3 signals. In the end, our data provide evidence for use of ouabain as a combination therapeutic with miR-34a against lung cancer and similar cancers with loss of miR-34a. These data will serve as a strong basis for future preclinical trials involving miR-34a treatment in lung cancer.

METHODS

All methods can be found in the accompanying Transparent Methods supplemental file.

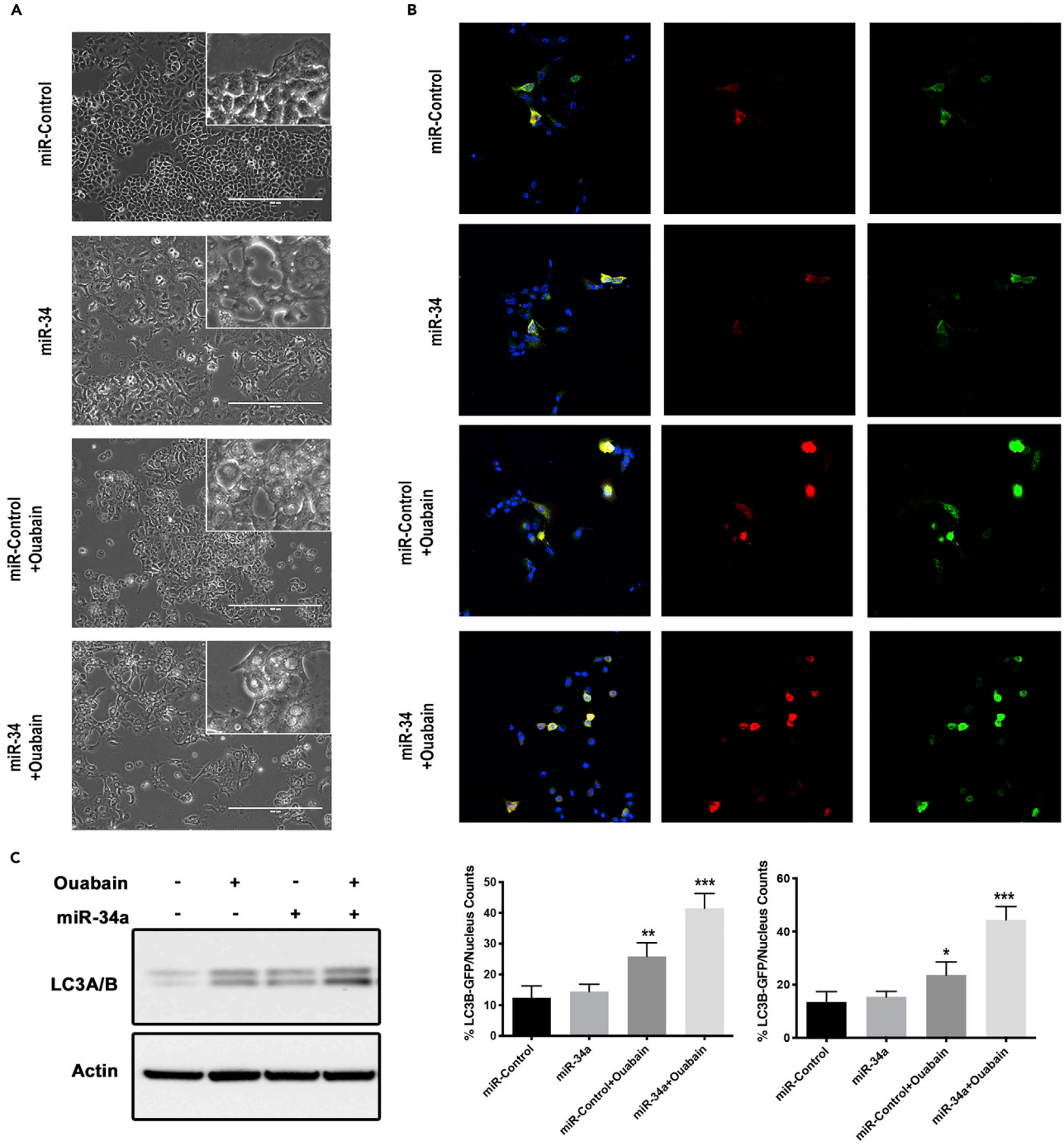

Figure 5. Ouabain and miR-34a Treatment Augments Autophagy in Cancer Cells

(A) Phase contrast images of A549 cells treated with miR-Control, miR-34a, ouabain, and combination of miR-34a (40 nM) with ouabain (IC50, 30 nM). All images are taken at 200× magnification. Images from cell treated with ouabain or miR-34a combination show large vacuoles, consistent with an autophagic phenotype.

(B) Fluorescent images from A549 cells with the RFP-GFP-LC3B reporter assay for autophagy. Autophagosomes (green) and LC3B-positive autophagolysosome (red) and nucleus (blue) are shown with quantification of number of respective positive cells as a percentage of total number of cells (lower panel).

(C) Western blot data showing LC3A/B bands in cells treated with miR-control, ouabain (30 nM), or miR-34a (40 nM) combinations in A549 cells. *$p < 0.05$, **$p < 0.01$, ***$p < 0.001$, Student's t test. Bars and errors bars represent the means and the corresponding SEMs for $n \geq 3$.

SUPPLEMENTAL INFORMATION

Supplemental Information can be found online at https://doi.org/10.1016/j.isci.2020.100878.

ACKNOWLEDGMENTS

This work was supported, in part, by the NIH-YALE SPORE in Lung Cancer P50CA196530 and the NCI Outstanding Investigator Award (R35CA232105). Additional support to F.J.S. was provided by the P50CA196530-03S1 and support from the Ludwig Center at Harvard. R.R. was supported by a Hope funds for Cancer Research postdoctoral fellowship. W.C.Z. was supported by NIH-YALE SPORE in Lung Cancer Career Development Program Award and NRSA 5T32HL007893-20.

AUTHOR CONTRIBUTIONS

R.R. designed the study and performed experiments, analyzed data, and wrote the manuscript. B.Y. and W.C.Z. participated in *in vitro* studies. B.D.A. provided the miR-34a expression plasmid system. F.J.S. designed and supervised the study and participated in manuscript preparation. All authors edited and approved the final manuscript.

DECLARATION OF INTERESTS

F.J.S. discloses financial interests and SAB roles with Mira DX and MiRNA Therapeutics. The other authors declare no competing interests.

Received: November 22, 2019
Revised: January 14, 2020
Accepted: January 28, 2020
Published: February 21, 2020

SUPPORTING CITATIONS

The following reference appears in the Supplemental Information: Adams et al., 2016; Di Veroli et al., 2016; Zhang et al., 2019.

REFERENCES

Adams, B.D., Wali, V.B., Cheng, C.J., Inukai, S., Booth, C.J., Agarwal, S., Rimm, D.L., Gyorffy, B., Santarpia, L., Pusztai, L., et al. (2016). miR-34a silences c-SRC to attenuate tumor growth in triple-negative breast cancer. Cancer Res. *76*, 927–939.

Bader, A.G. (2012). miR-34 – a microRNA replacement therapy is headed to the clinic. Front. Genet. *3*, 120.

Bartel, D.P. (2004). MicroRNAs. Cell *116*, 281–297.

Beg, M.S., Brenner, A., Sachdev, J., Ejadi, S., Borad, M., Kang, Y.-K., Lim, H., Kim, T.-Y., Bader, A., Stoudemire, J., et al. (2015). Abstract C43: safety, tolerability, and clinical activity of MRX34, the first-in-class liposomal miR-34 mimic, in patients with advanced solid tumors. In Clinical Trials (American Association for Cancer Research), p. C43.

Chang, T.-C., Wentzel, E.A., Kent, O.A., Ramachandran, K., Mullendore, M., Lee, K.H., Feldmann, G., Yamakuchi, M., Ferlito, M., Lowenstein, C.J., et al. (2007). Transactivation of miR-34a by p53 broadly influences gene expression and promotes apoptosis. Mol. Cell *26*, 745–752.

Cherniavsky-Lev, M., Golani, O., Karlish, S.J.D., and Garty, H. (2014). Ouabain-induced internalization and lysosomal degradation of the Na +/K + -ATPase. J. Biol. Chem. *289*, 1049–1059.

Di Veroli, G.Y., Fornari, C., Wang, D., Mollard, S., Bramhall, J.L., Richards, F.M., and Jodrell, D.I. (2016). Combenefit: an interactive platform for the analysis and visualization of drug combinations. Bioinformatics *32*, 2866–2868.

Kasinski, A.L., and Slack, F.J. (2012). miRNA-34 prevents cancer initiation and progression in a therapeutically resistant K-ras and p53-induced mouse model of lung adenocarcinoma. Cancer Res. *72*, 5576–5587.

Kasinski, A.L., Kelnar, K., Stahlhut, C., Orellana, E., Zhao, J., Shimer, E., Dysart, S., Chen, X., Bader, A.G., and Slack, F.J. (2015). A combinatorial microRNA therapeutics approach to suppressing non-small cell lung cancer. Oncogene *34*, 3547–3555.

Li, L., Yuan, L., Luo, J., Gao, J., Guo, J., and Xie, X. (2013). MiR-34a inhibits proliferation and migration of breast cancer through down-regulation of Bcl-2 and SIRT1. Clin. Exp. Med. *13*, 109–117.

Liu, C., Kelnar, K., Liu, B., Chen, X., Calhoun-Davis, T., Li, H., Patrawala, L., Yan, H., Jeter, C., Honorio, S., et al. (2011). The microRNA miR-34a inhibits prostate cancer stem cells and metastasis by directly repressing CD44. Nat. Med. *17*, 211–215.

Misso, G., Di Martino, M.T., De Rosa, G., Farooqi, A.A., Lombardi, A., Campani, V., Zarone, M.R., Gullà, A., Tagliaferri, P., Tassone, P., et al. (2014). Mir-34: a new weapon against cancer? Mol. Ther. *3*, e195.

Orellana, E.A., Tenneti, S., Rangasamy, L., Lyle, L.T., Low, P.S., and Kasinski, A.L. (2017). FolamiRs: ligand-targeted, vehicle-free delivery of microRNAs for the treatment of cancer. Sci. Transl. Med. *9*, eaam9327.

Parzych, K.R., and Klionsky, D.J. (2014). An overview of autophagy: morphology, mechanism, and regulation. Antioxid. Redox Signal. *20*, 460–473.

Peng, Y., and Croce, C.M. (2016). The role of MicroRNAs in human cancer. Signal. Transduct. Target. Ther. *1*, 15004.

Reinhart, B.J., Slack, F.J., Basson, M., Pasquinelli, A.E., Bettinger, J.C., Rougvie, A.E., Horvitz, H.R., and Ruvkun, G. (2000). The 21-nucleotide let-7 RNA regulates developmental timing in *Caenorhabditis elegans*. Nature *403*, 901–906.

Rupaimoole, R., and Slack, F.J. (2017). MicroRNA therapeutics: towards a new era

for the management of cancer and other diseases. Nat. Rev. Drug Discov. *16*, 203–222.

Siegel, R.L., Miller, K.D., and Jemal, A. (2019). Cancer statistics, 2019: cancer statistics, 2019. CA. Cancer J. Clin. *69*, 7–34.

Stahlhut, C., and Slack, F.J. (2015). Combinatorial action of MicroRNAs let-7 and miR-34 effectively synergizes with erlotinib to suppress non-small cell lung cancer cell proliferation. Cell Cycle *14*, 2171–2180.

Trang, P., Wiggins, J.F., Daige, C.L., Cho, C., Omotola, M., Brown, D., Weidhaas, J.B., Bader, A.G., and Slack, F.J. (2011). Systemic delivery of tumor suppressor microRNA mimics using a neutral lipid emulsion inhibits lung tumors in mice. Mol. Ther. *19*, 1116–1122.

Trenti, A., Grumati, P., Cusinato, F., Orso, G., Bonaldo, P., and Trevisi, L. (2014). Cardiac glycoside ouabain induces autophagic cell death in non-small cell lung cancer cells via a JNK-dependent decrease of Bcl-2. Biochem. Pharmacol. *89*, 197–209.

Zhang, W.C., Wells, J.M., Chow, K.-H., Huang, H., Yuan, M., Saxena, T., Melnick, M.A., Politi, K., Asara, J.M., Costa, D.B., et al. (2019). miR-147b-mediated TCA cycle dysfunction and pseudohypoxia initiate drug tolerance to EGFR inhibitors in lung adenocarcinoma. Nat. Metab. *1*, 460–474.

iScience, Volume *23*

Supplemental Information

A High-Throughput Small Molecule Screen Identifies Ouabain as Synergistic with miR-34a in Killing Lung Cancer Cells

Rajesha Rupaimoole, Bohyung Yoon, Wen Cai Zhang, Brian D. Adams, and Frank J. Slack

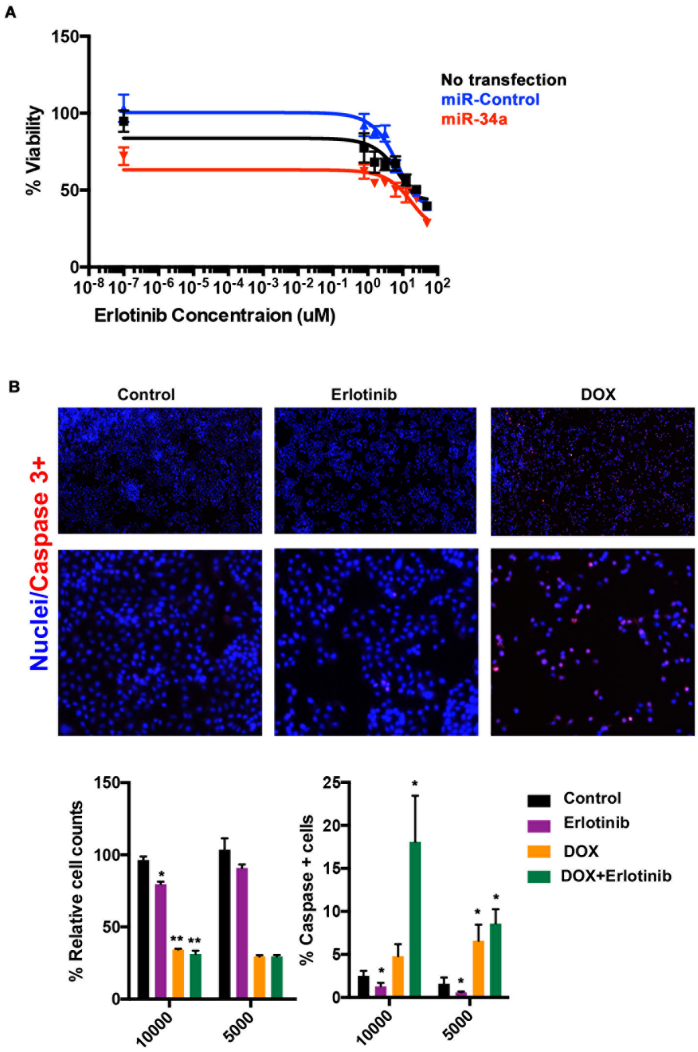

Supplemental Figure 1: Standardization of the assay for measuring cell number and caspase activity after treating cells with miR-34a and small molecules. Related to Figure 2. **A)** Viability curves from A549 cells treated with miR-34a compared to controls and increasing doses of erlotinib. B) Nuclei stained using Hoechst 33342 and activated caspase 3 positive cells stained using Nucview 549, images were taken at 200x. The top panel shows A549 cells treated with miR-control, miR-34a, erlotinib or combination of miR-34a and erlotinib. The bottom panel shows quantified data from nuclei and activated caspase 3 positive cell counts in two different cell plating conditions. *p<0.05, **p<0.01, Student's t test. Bars and errors bars represent the means and the corresponding SEMs for $n \geq 3$

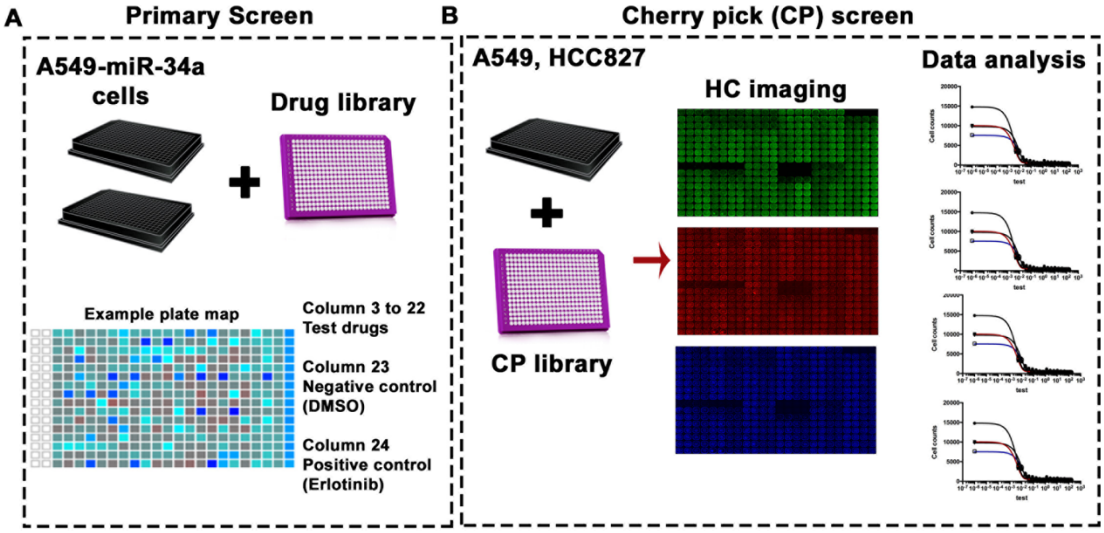

Supplemental Figure 2: Outline of the high throughput screen. Related to Figure 3. A) Schematic of the primary screen with A549 cells with expression of miR-34a, under the control of the tetracycline responsive element. A plate map of screen setup is shown. B) An outline of the cherry pick screen and identification of top candidate molecules to combine synergistically with miR-34a is shown.

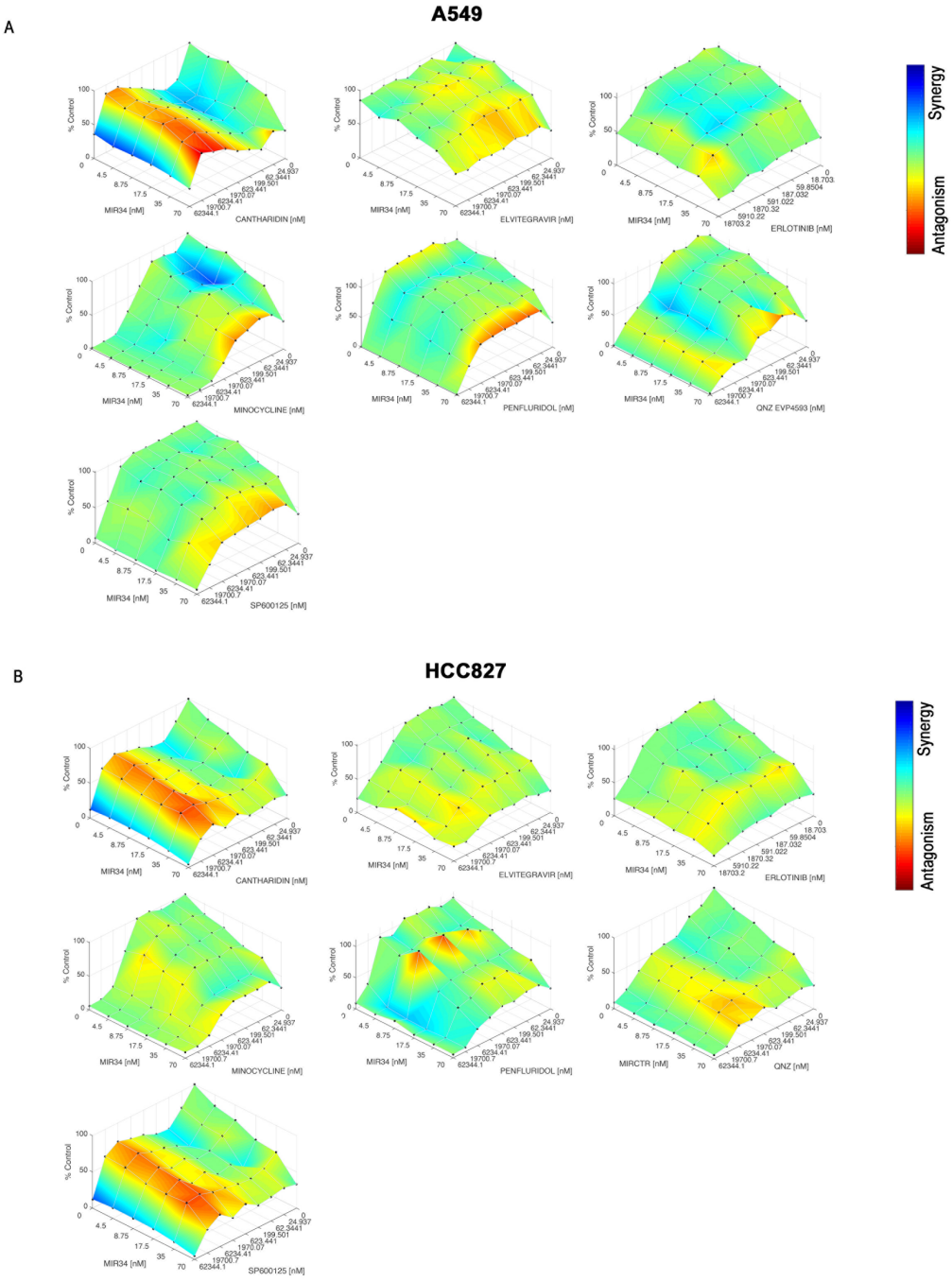

Supplemental Figure 3: Synergy plots of miR-34a and the top 8 molecules in treated lung cancer cells A549 (A) and HCC827 (B). Related to Figure 3. Lowe's additivity combination index was calculated and plotted as heatmap using Combenefit data analysis tool.

Supplemental Tables

Name of the Library	Description (Source: ICCB-Longwood)
NIH Clinical Collection 1 and 2	This collection was assembled by the National Institutes of Health (NIH) and is comprised of molecules that have a history of use in human clinical trials
Microsource1	These have reached clinical trial stages in the USA. Each compound has been assigned USAN or USP status and is included in the USP Dictionary
LOPAC1	Collection of 1280 pharmacalogically-active compounds from Sigma, USA
Biomol4	Known and well-characterized bioactivities and undergone safety and bioavailability testing
MSDiscovery1	This is a collection of compounds newly available at MicroSource (part of their Pharmakon 1600 library) and not previously represented in ICCB-L Known Bioactives libraries
Selleck-3.33mM	This library contains some FDA-approved compounds and most of Selleck's inhibitors, active pharmaceutical agents, and chemotherapeutic agents
eMolecules	Small molecules included in this library were identified via text mining from a variety of sources including ChEMBL, ClinicalTrials and DrugBank by chemists at eMolecules
Prestwick2 Collection	This library contains 1120 off-patent compounds that have been selected for structural diversity, collective coverage of multiple therapeutic areas, and known safety and bioavailability in humans
Cayman Biolipid	Included are prostaglandins, thromboxanes, cannabinoids, D-myo–inositol-phosphates, phosphatidylinositol-phosphates, sphingolipids, inhibitors, receptor agonists and antagonists, ceramide derivatives, and several other complex polyunsaturated fatty acids
Biomol ICCB known bioactives	The collection includes many classes of compounds including ion channel blockers, GPCR ligands, second messenger modulators, nuclear receptor ligands, actin and tubulin ligands, kinase inhibitors, protease inhibitors, gene regulation agents, lipid biosynthesis inhibitors
Tocriscreen MiniLibrary	A collection of 1120 biologically active compounds
Chembridge KINAcore	These molecules have total of 34 targets (ADK, Aurora, BRAF, CDK, CDK2, CDK5, CHK1, C-MET, CSFR1, EGFR, FGFR, GRK2, GSK, HER, IKK, IRAK, JAK, JNN, LCK, MYT-1, P38 MAP, PDGFR, PI3K, PKA, PKB, PKC, PLK1, RAF, SRC, SYK, TGFR, TIE2, TK, VEGFR) by 16 different scaffolds, with each scaffold having a minimum of 5 targets

Supplemental Table 1: List of compound libraries used in the study and content description of each of the library set from ICCB-Longwood small molecule screening facility. Related to Figure 3

Number	Compound Names	Fold change		Number	Compound Names	Fold change	
		Total cell counts	Caspase 3+ counts			Total cell counts	Caspase 3+ counts
1	SDM25N	0.2446	1.9599	26	Doxycycline hyclate	0.6408	1.7633
2	Pyrithione zinc	0.4158	2.9319	27	WHI-P154	0.645	0.9309
3	Digitoxin	0.4238	1.5281	28	Pimozide	0.645	0.9095
4	Doxifluridine	0.4508	2.0884	29	Quinacrine	0.6483	1.6384
5	Ftorafur	0.4627	3.7194	30	SP-600125	0.6549	1.6197
6	L-703,606 Oxalate	0.4845	0.2814	31	Dioscin	0.658	1.3874
7	Cladribine	0.4854	5.5569	32	(R)-SLV 319	0.6628	0.4677
8	Clofazimine	0.5146	1.3694	33	5-Nonyloxytryptamine	0.6638	1.9585
9	Ouabain	0.5365	2.2016	34	T 0070907	0.6671	2.8365
10	Azacitidine	0.5556	2.9755	35	SNAP 5089	0.6678	1.8827
11	Terfenadine	0.562	4.339	36	BVT 948	0.6719	1.772
12	Bay 11-7821	0.5682	4.0154	37	Phorbol	0.6758	1.6242
13	Darapladib	0.5774	1.5815	38	Penfluridol	0.6767	1.1929
14	Mibefradil	0.5822	0.6806	39	Ionomycin	0.6794	0.9221
15	3,4-DAA	0.5849	0.6874	40	Xylazine HCl	0.6807	1.3269
16	Go6976	0.5909	1.0553	41	PFK15	0.6814	0.506
17	Cantharidin	0.5923	2.5958	42	QNZ EVP4593	0.6834	3.233
18	Lanatoside c	0.5998	2.3108	43	Meclocycline	0.6838	2.9329
19	Tannic acid	0.6021	1.4585	44	Minocycline HCl	0.6889	1.8871
20	HMB-Val-Ser-Leu-VE	0.6096	0.7812	45	ARQ 621	0.6895	0.42
21	Elvitegravir	0.6108	1.2621	46	NNC 05-2090 Hcl	0.6939	1.5537
22	Cetrimonium Bromide	0.6155	3.2117	47	Stattic	0.6976	0.9635
23	Sertraline hydrochloride	0.6205	0.9981	48	GSK J4 HCl	0.6982	1.3702
24	Nifedipine	0.6242	1.7792	49	1-Linoleoyl Glycerol	0.6983	0.4773
25	Lacidipine	0.6353	1.5741	50	PD 158780	0.6988	1.7043

Supplementary Table 2: Molecules used in cherry pick screen along with the % change in total cell counts and caspase 3+ cell counts. Comparison was done between control cells and miR-34a induced cells. Related to Figure 3.

Drug name	Growth inhibition 30 (GI30)		% Decrease in GI30	Increase in Caspase 3+ cells
	DMSO Control	DOX +		
Minocycline HCl	14.15	1.42	89.96466431	Yes
Digitoxin	0.062	0.017	72.58064516	Yes
Ouabain	0.021	0.003	85.71428571	Yes
Meclocycline	9.63	2.882	70.07268951	Yes
Cantharidin	2.479	0.734	70.39128681	Marginal
Doxycycline	13.62	4.539	66.67400881	Yes
Mibefradil	13.177	4.958	62.37383319	Marginal
Phorbol	30.858	0.009	99.97083414	Yes
Penfluridol	33.22	4.832	85.45454545	Yes
SP-600125	19.548	3.62	81.48148148	Yes
T 0070907	33.22	11.442	65.55689344	Marginal
Nifedipine	35.5	12.029	66.11549296	Yes
Lacidipine	33.22	7.254	78.16375677	Yes
QNZ - EVP4593	10.776	2.954	72.58723088	Yes
Elvitegravir	3.811	0.819	78.50957754	Yes

Supplementary Table 3: List of molecules used in combination index calculations. GI30 calculated from dose response of individual drugs selected from cherry pick screen. Related to Figure 3.

Transparent Methods

Cell line maintenance, microRNA mimic transfections, and establishing cell lines for screen

All cell lines used in the study were maintained in 5% CO2, 37^0 C standard cell culture incubators, with weekly media change and close monitoring. All the cell lines used in the study were obtained from American type cell culture collection (ATCC) and maintained in RPMI1640 medium supplemented with 15% FBS and antibiotics. All cell lines were routinely tested for mycoplasma. Lung cancer patient derived xenograft (PDX) was obtained and processed as previously discussed (Zhang et al., 2019). All research involving PDX studies were granted ethical approval by the Beth Israel Deaconess Medical Center. Prior to miRNA transfections, spheroid cultures were established from PDX primary cultures in geltrex (Gibco) as support matrix (25 µl/well) mixed with complete growth media (20 µl/well) in 96-well non-treated clear plates (Corning). The complete growth media composition is published previously (Zhang et al., 2019). For each 96 wells containing spheroids, 10^3 cells were plated in the above mixture of Matrigel and media, incubated for 7 days before transfection with miRNA control and miR-34a as per below protocol.

For miRNA transfections, RNAiMAX Lipofectamine (Life Technologies) was used as a transfection agent, and the ratio of RNAiMAX to a specific miRNA was 2:1 (nM to ul). The concentration of miRNAs used for transfection was set to 40nM. Briefly, miRNA mimics for miR-34a and control miRNA (Life Technologies) were diluted in Opti-MEM media and liposomal complex was prepared by adding RNAiMAX reagent. The mixture was incubated for 15 min before adding to the cell mixture in complete media and incubated for the specific time frame of the studies mentioned below.

For the small molecule screen, A549 and HCC827 cells were transduced with lentiviral particles containing miR-34a overexpression system under tight control of a tetracycline responsive element (TET, doxycycline inducible). Using constitutive eGFP, cells were selected in two rounds for actively transduced cells. For inducing miR-34a expression, doxycycline (Sigma Aldrich) was added at different doses in 6 well plate cultures of A549 and HCC827 cells previously transduced with lentiviral particles containing miR-34a over expression plasmid. Using qPCR, induction of miR-34a expression and downstream target CD44 (Liu et al., 2011) and SRC (Adams et al., 2016) mRNA changes were measured.

High-throughput screen (HTS) to identify miR-34a synergistic small compounds

HTS was standardized and performed against 9908 small molecule compounds which are part of biologically active small molecule collection at the ICCB Longwood screening facility (Harvard Medical School). In 384 well plates, assays to count the total number of cells and activated caspase using Nucview 549 probe (Biotium) were standardized. As a positive control, Erlotinib at IC50 dose for A549 cells was used in every screening plate (two replicates per compound). Post plating A549-miR-34a cells with 1 ug/ml of doxycycline, compounds were transferred to individual wells using a pin-transfer system, and the plates were incubated at 37°C in 5% CO_2 for 72 hr. After the incubation period, cell plates were removed, washed with PBS and incubated with Hoechst 33342 (Thermofisher) and Nucview 549 (Biotium) for 10min and cells were fixed with 4% paraformaldehyde. Signals from each well were quantified

using Acumen eX3 high content imager (TTPLabtech) and data plotted as % total cells and % caspase positive cells compared to control DMSO treatments. The Z-factor was used for quality control purposes and each plate's positive control and negative control readings were used for calculations. A Z-factor of 0.5 was used as cutoff for quality control of each plate and assay. The top 10% of compounds with the highest decrease in viability and further cutoff of an increase in caspase 3+ cells (n=58) were used for a cherry pick screen with a dose response curve. Further combination index analysis on the top selected candidates were performed with miR-34a or miR-control at increasing doses in a matrix of increasing dose of compounds. Data analysis using Combenefit (Di Veroli et al., 2016) tool with Loews additivity combination calculations were carried out. The top two compound with significant synergy points were used for further analysis. Raw data from the screen deposited at Pubchem with AID 1347080.

Immunoblotting and Quantitative real-time PCR

For Western blotting, lysates from cultured cells were prepared using modified RIPA buffer (50 mM Tris–HCl (pH 7.4), 150 mM NaCl, 1% Triton, 0.5% deoxycholate) plus Halt phosphatase and protease inhibitor cocktail (Pierce Biotechnology) at 1x concentration. The protein concentrations were determined using a BCA Protein Assay Reagent kit (Pierce Biotechnology). Lysates were loaded and separated on SDS–PAGE. Proteins were transferred to a nitrocellulose membrane by semidry electrophoresis (Bio-Rad Laboratories) overnight, blocked with 5% BSA for 1 h and then incubated at 4 °C overnight with primary antibody against LC3A/B 1:500 (Novus Biologicals). After washing with TRIS-buffered saline with Tween 20, the membrane was incubated with horseradish peroxidase-conjugated horse anti-Mouse or Rabbit IgG (1:2,000, GE Healthcare) for 2 h. Horseradish peroxidase was visualized using an enhanced chemiluminescence detection kit (Pierce Biotechnology). To confirm equal sample loading, the blots were probed with an antibody specific for β-actin (0.1 μg ml^{-1}; Sigma).

For mRNA and miRNA quantification, total RNA was isolated using the Direct-zol™ RNA MiniPrep Plus kit following the manufacturer protocol (Zymo Research). For mRNA measurements, 1,000 ng of RNA was used to synthesize complementary DNA using a Verso cDNA kit (Thermo Scientific), as per the manufacturer's instructions. Analysis of mRNA levels was performed on a Roche 384 Real-Time PCR System (Roche) using pre-validated (Qiagen) primers specific for each of the genes. Semi-quantitative real-time PCR was done with reverse-transcribed RNA and 100 ng μl^{-1} sense and antisense primers in a total volume of 10 μl. For miRNA quantification TaqMan miRNA assays (Life Technologies) were used and reverse transcription, real-time PCR were carried out, according to the manufacturer's instructions. *RNU6B* (for mature miRNAs) or *18S* (mRNAs) were used as a housekeeping gene.

Detection of autophagy in miR-34a and ouabain treated cells

Measurement of autophagy in cells treated with control miRNA and miR-34a with or without ouabain was carried out using the Premo™ Autophagy Tandem Sensor RFP-GFP-LC3B Kit (Thermo Fisher Scientific) as described in the manufacturer's instructions. The RFP-GFP-LC3B sensor enables the detection of LC3B positive, neutral pH autophagosomes in green fluorescence (GFP) and LC3B positive acidic pH autophagolysosome in red fluorescence (RFP). The cells were grown on chamber slides with transfection of miR-34a or miR-control. Following transfections,

cells were treated with ouabain (30nM) or DMSO control and incubated with BacMam Reagents containing the RFP-GFP-LC3B overnight. Treatment was done for total of 24hrs and cells were washed with PBS, nuclei were stained with Hoechst 33342. Fluorescent images were taken using confocal microscopy (Carl Zeiss Meditec). LC3B positive autophagosomes (green) and LC3B positive autophagolysosome (red) were analyzed as ratio of percentage of RFP and GFP positive cells compared total cells per field (200x).

Statistics

For all the data presented, graphs were plotted using Prism (Graphpad Software). For all statistical comparisons, Student's t test or ANOVA were used with multiple comparison tests. P value for significance was set at minimum of 0.05. Data is representative of triplicate experiments, unless otherwise mentioned in figure legends.